Supporting Information

Twisted Schiff-base macrocycle showing excited-state intramolecular proton-transfer (ESIPT): assembly and sensing properties

Qing Yu, Xiaodong Zhang, Shou-Ting Wu, Huaiyu Chen, Qi-Long Zhang, Hong Xu, Ya-Li Huang, Bi-Xue Zhu and Xin-Long Ni

Synthesis of the hemi-**MH** (**L**): 5,5′-methylene-bis-salicylaldehyde (256.0 mg, 1 mmol) and phenylamine (93.0 mg, 1 mmol) were dissolved in methanol solution (40.0 mL) in a round bottomed flask for 10 min, and conc. H_2SO_4 (12 μL) was added to the solution. The resulting mixture was stirred at room temperature for 4 h. Then, the reaction mixture was filted to give the crude solid product, and the residue was washed with methanol three times to afford a light yellow solid compound **L** (345 mg, 85%). Single crystals were obtained from a crystal grown by evaporation of **L** (50.0 mg) in a solution of $CHCl_3$. CCDC1969906. ^{1}H NMR (400 MHz, DMSO-d_6) δ 12.88 (s, 2H), 8.87 (s, 2H), 7.47 (d, J = 16 Hz, 2H), 7.41 (s, 2H), 7.39 (d, J = 12 Hz, 4H), 7.34 (d, J = 8 Hz, 4H), 7.30-7.22 (m, 6H), 6.88 (d, J = 12Hz, 2H), 3.87 (s, 2H) ppm.^{13}C NMR (100 MHz, DMSO-d_6) δ 163.84, 159.14, 148.68, 134.34, 132.60, 132.49, 129.99, 127.45, 121.90, 119.66, 117.25, 39.36 ppm.

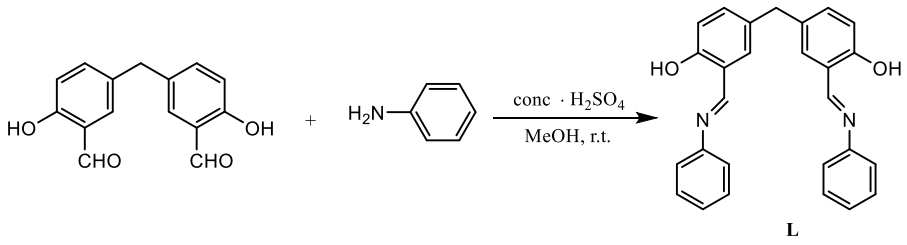

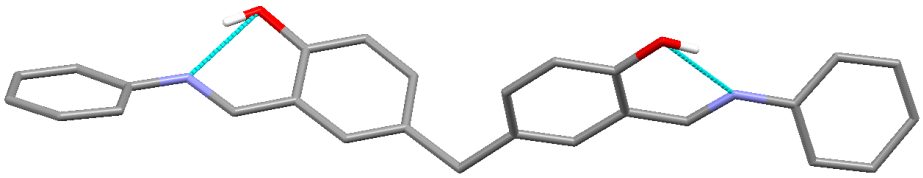

Scheme S1 Synthetic route to the hemi-MH (**L**), and the X-ray structure.

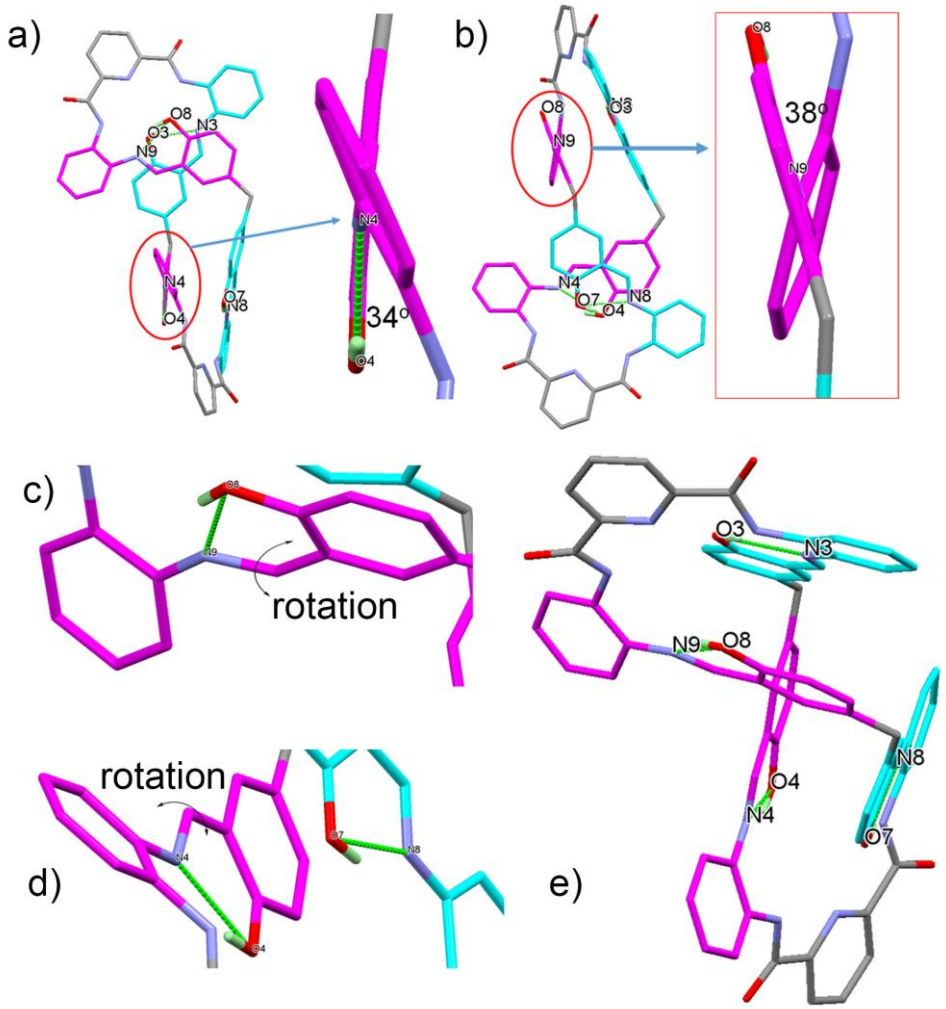

Fig. S1 X-ray structure of **MH**: (a) dihedral angle between C3 and C4 linked by hydrogen bonds O4-N4, (b) dihedral angle between C3 and C4 linked by hydrogen bonds O8-N9, (c, d) plausible rotation tendency between the C3 and C4, (e) top view of the coplanar arrangement of C1 and C2.

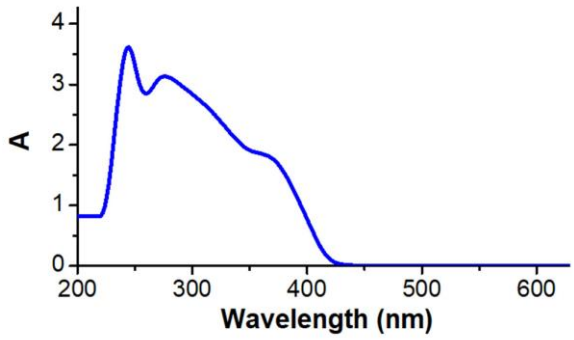

Fig. S2 UV-vis absorption spectra of **MH** (20.0 μM) in THF solution.

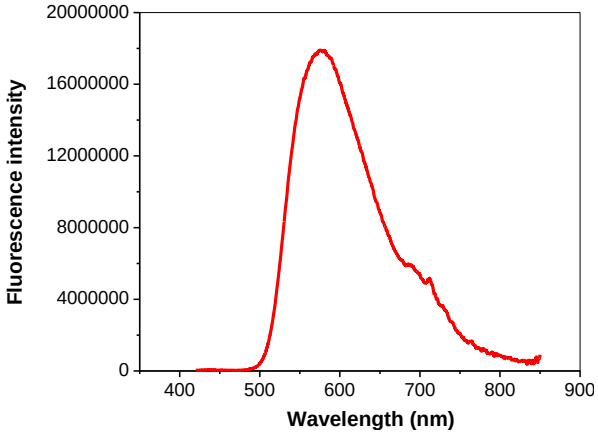

Fig. S3 Fluorescence spectra of **MH** in the solid state. (λ_{ex} = 395 nm)

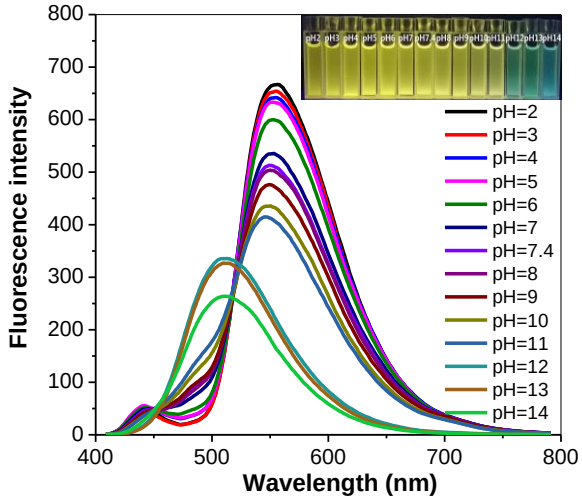

Fig. S4 Fluorescence spectra of **MH** (20.0 μM) in the range from pH = 2 to 14 in THF/water solution (1:1, v/v). (λ_{ex} = 395 nm)

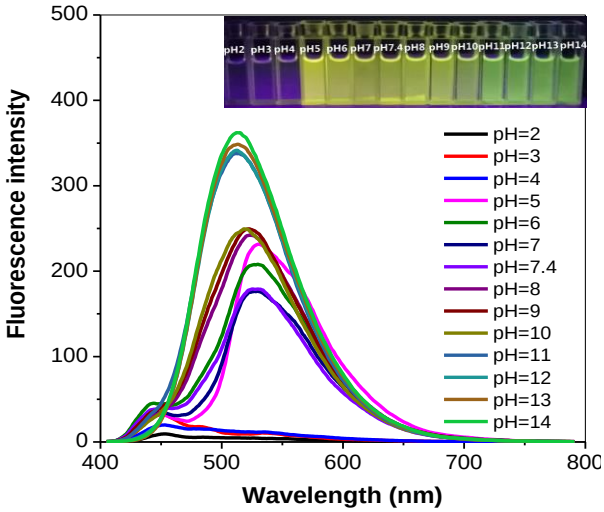

Fig. S5 Fluorescence spectra of **L** (20.0 μM) in the range from pH = 2 to 14 in THF/water solution (1:1, v/v). (λ_{ex} = 395 nm)

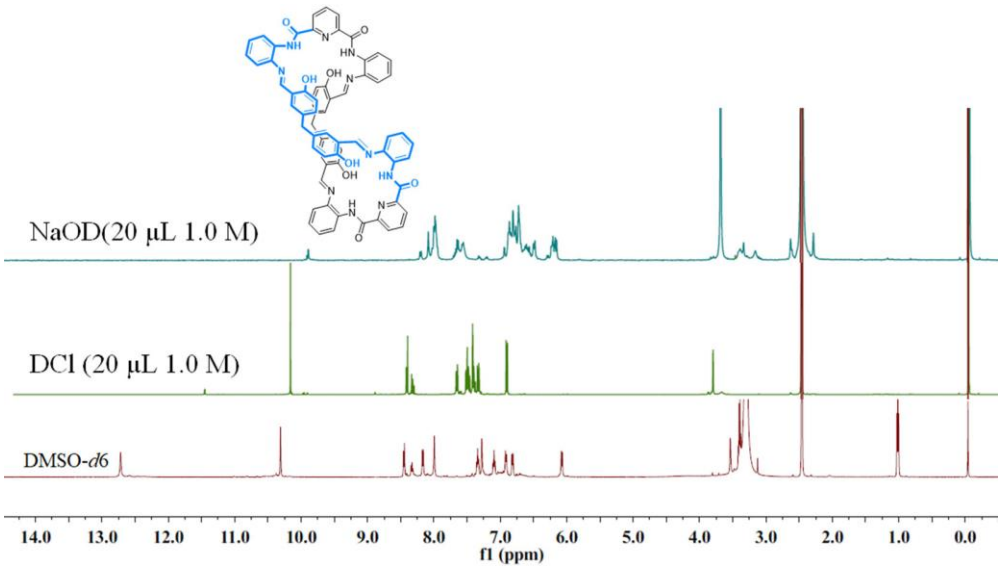

Fig. S6 ^{1}H NMR spectra of **MH** (1.0 mM, DMSO-*d*6) in the presence of DCl and NaOD.

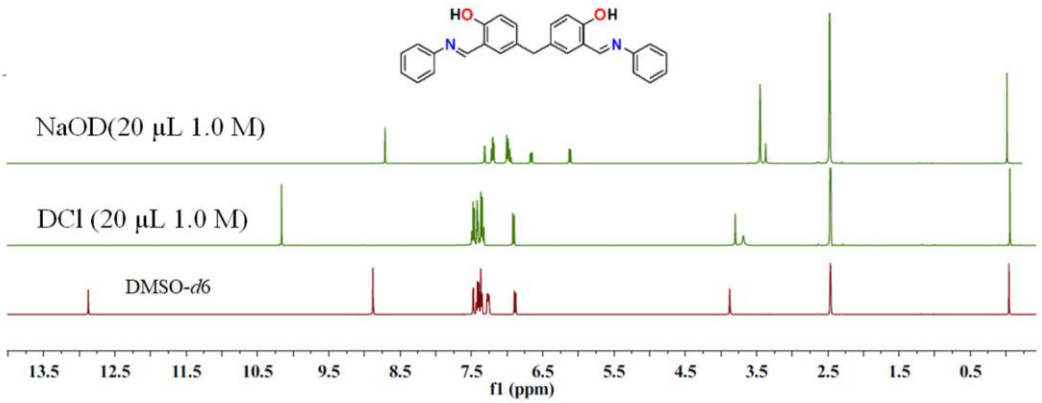

Fig. S7 ^{1}H NMR spectra of **L** (1.0 mM, DMSO-*d*6) in the presence of DCl and NaOD.

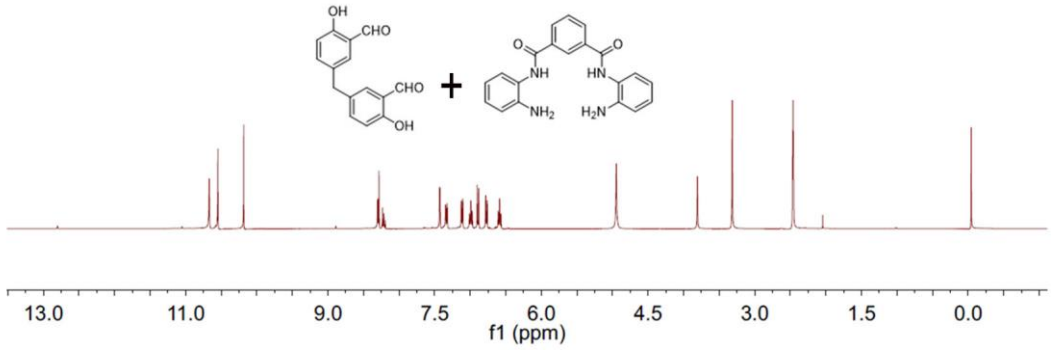

Fig. S8 ^{1}H NMR spectra (DMSO-*d*6) of the mixture precursors (aldehyde and amine) of **MH**.

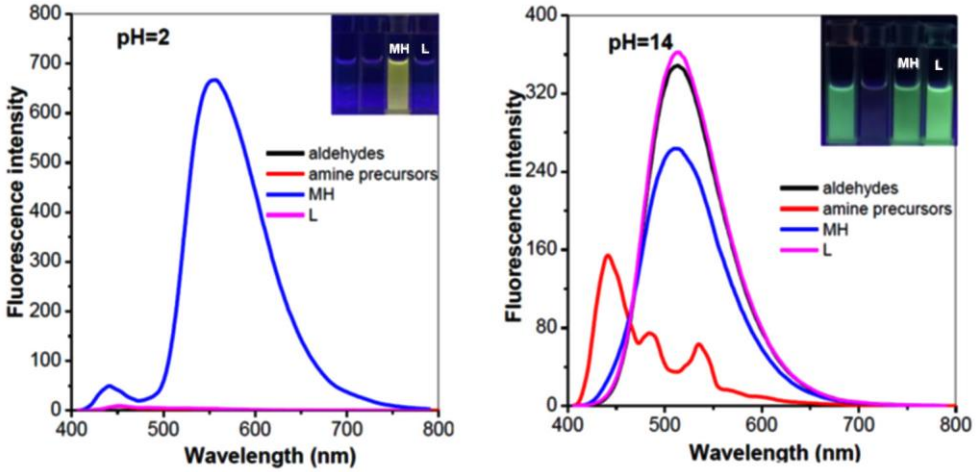

Fig. S9 Fluorescence spectra of **MH**, **L** and their precursors in THF/water solution (1:1, v/v) at pH 2.0 and pH 14, respectively.

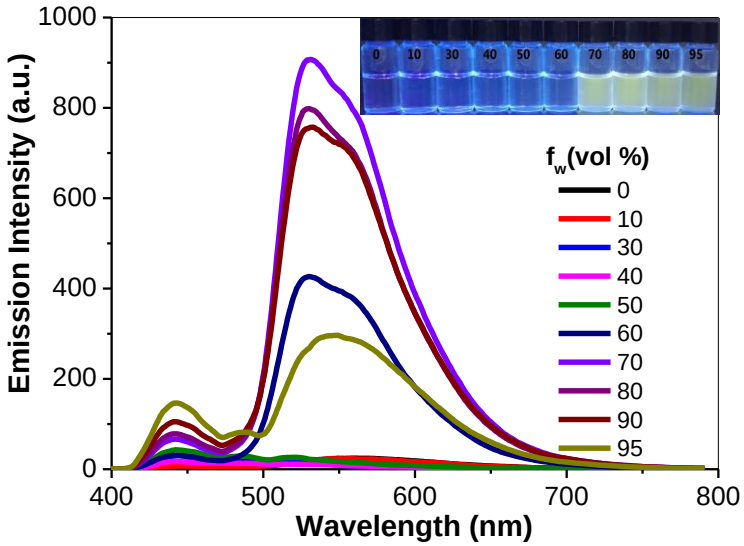

Fig. S10 Fluorescence spectra of **L** (20.0 μM) with different water fractions (f_w). (λ_{ex} = 395 nm)

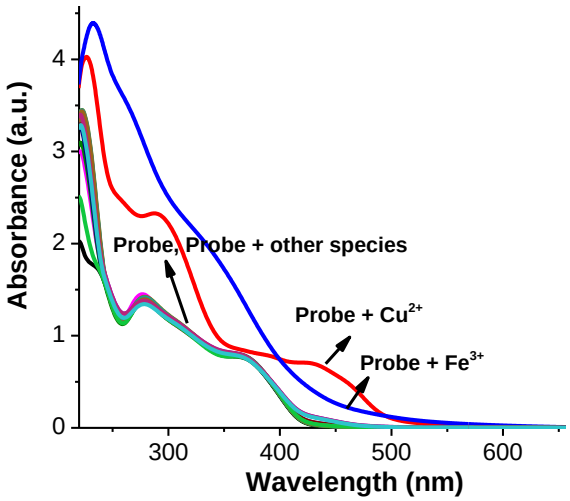

Fig. S11 UV-vis spectra of **MH** probe (20.0 μM) with addition of nitrate salts of Li^{+}, Co^{2+}, Cr^{3+}, K^{+}, Cd^{2+}, Pb^{2+},Ca^{2+}, Hg^{2+}, Ba^{2+}, Cu^{2+}, Mg^{2+}, Ni^{2+}, Zn^{2+}, Al^{3+} and Fe^{3+} (150 μM) in THF/water solution (1:4, v/v).

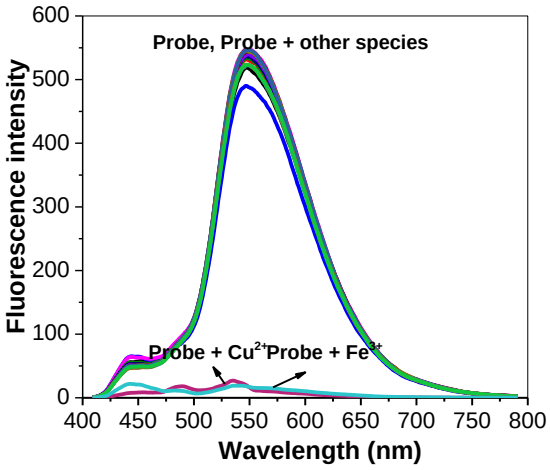

Fig. S12 Fluorescence spectra of **MH** probe (20.0 μM) with addition of nitrate salts of Li^{+}, Co^{2+}, Cr^{3+}, K^{+}, Cd^{2+}, Pb^{2+},Ca^{2+}, Hg^{2+}, Ba^{2+}, Cu^{2+}, Mg^{2+}, Ni^{2+}, Zn^{2+}, Al^{3+} and Fe^{3+} (150 μM) in THF/water solution (1:4, v/v). (λ_{ex} = 395 nm)

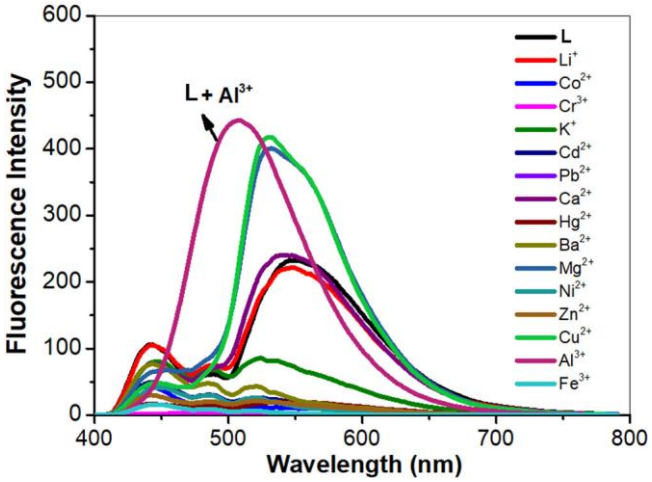

a)

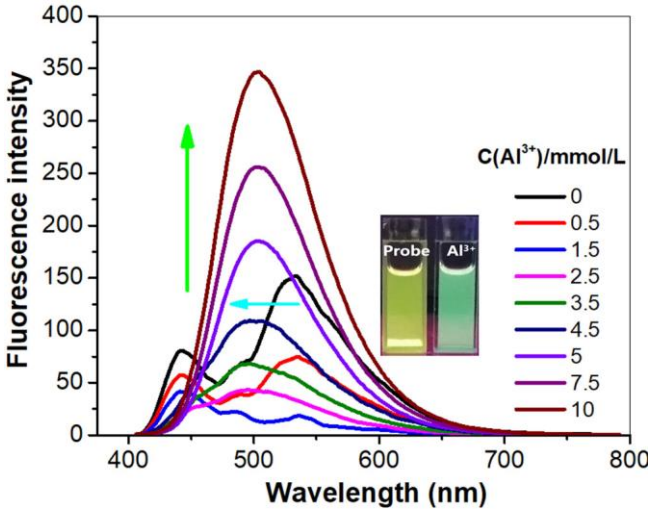

b)

Fig. S13 Fluorescence spectra of **L** probe (20.0 μM) in presence of various metal ions (150 μM) (a), and in the presence of increasing concentration of Al^{3+} ions in THF/water solution (1:1, v/v). (λ_{ex} = 395 nm)

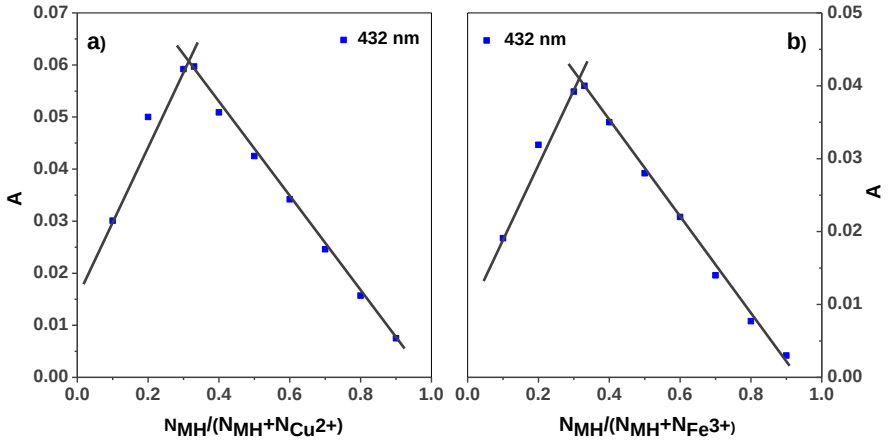

Fig. S14 Job plot of **MH** toward Cu^{2+}(a) and Fe^{3+}(b).

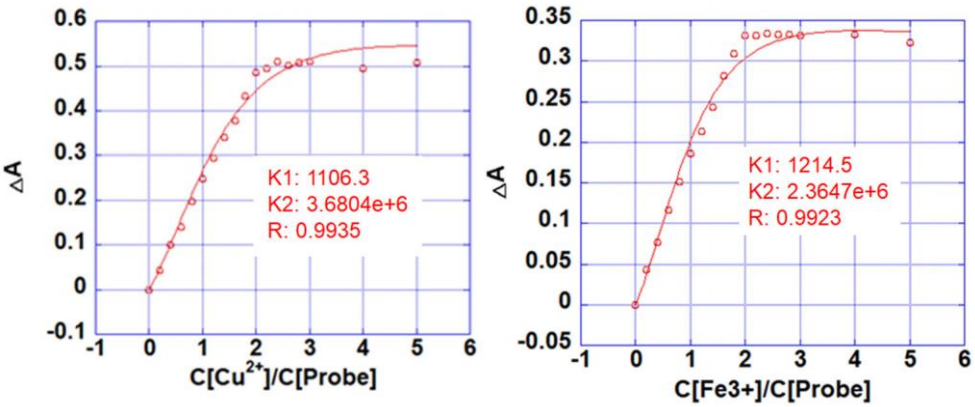

Fig. S15 The 1:2 binding constants (K_a) of MH with Cu^{2+} and Fe^{3+} was calculated (using the soft of KaleidaGraph 4.0) to be 1.10×10^3 M^{-1} and 3.68×10^6 M^{-1} for Cu^{2+} and 1.21×10^3 M^{-1}, and 2.36×10^6 M^{-1} for Fe^{3+}, respectively. The red solid line was obtained from the non-linear curve-fitting.

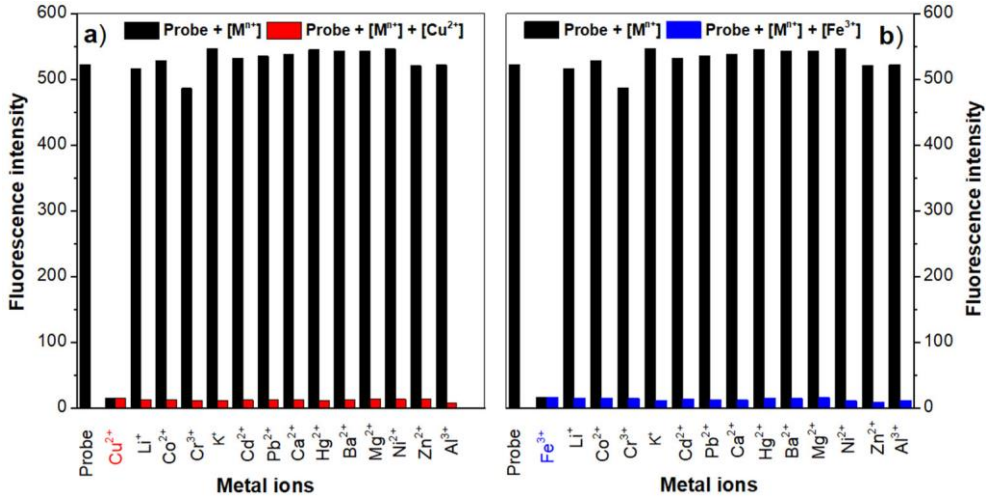

Fig. S16 Bar diagram of the competitive experiments of various metal cations on the fluorescence intensity of the probe / Cu^{2+} complex (a) and the probe / Fe^{3+} complex (b).

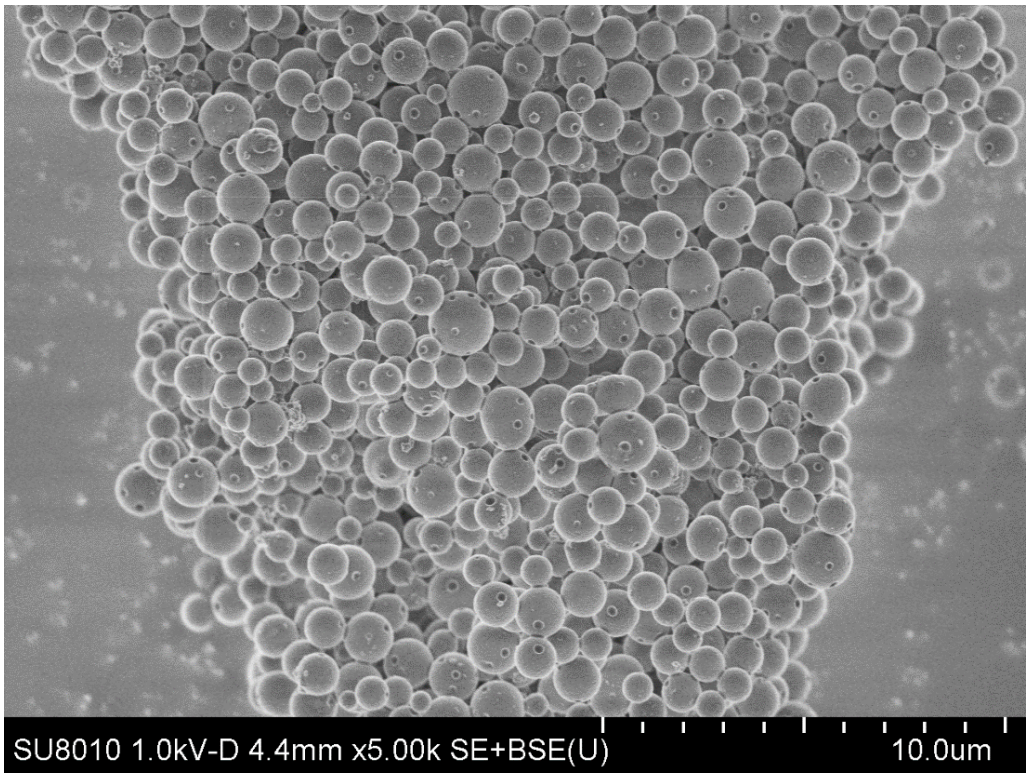

a)

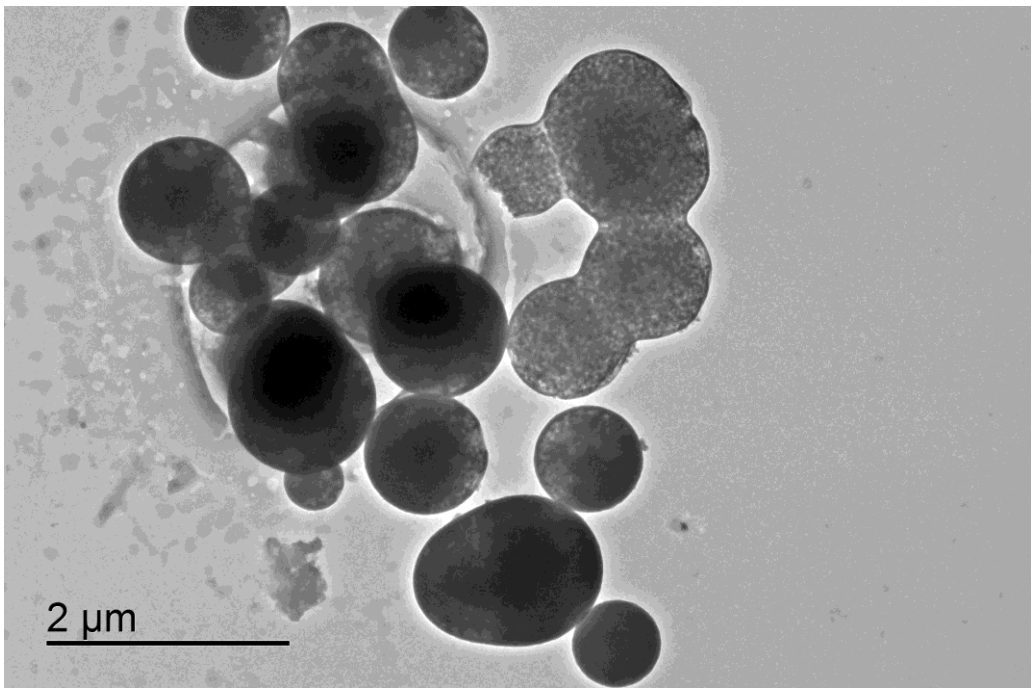

b)

Fig. S17 SEM (a) and TEM (b) images of the precipitate of **MH**/Fe^{3+} from THF/H_2O (1:4, v/v).

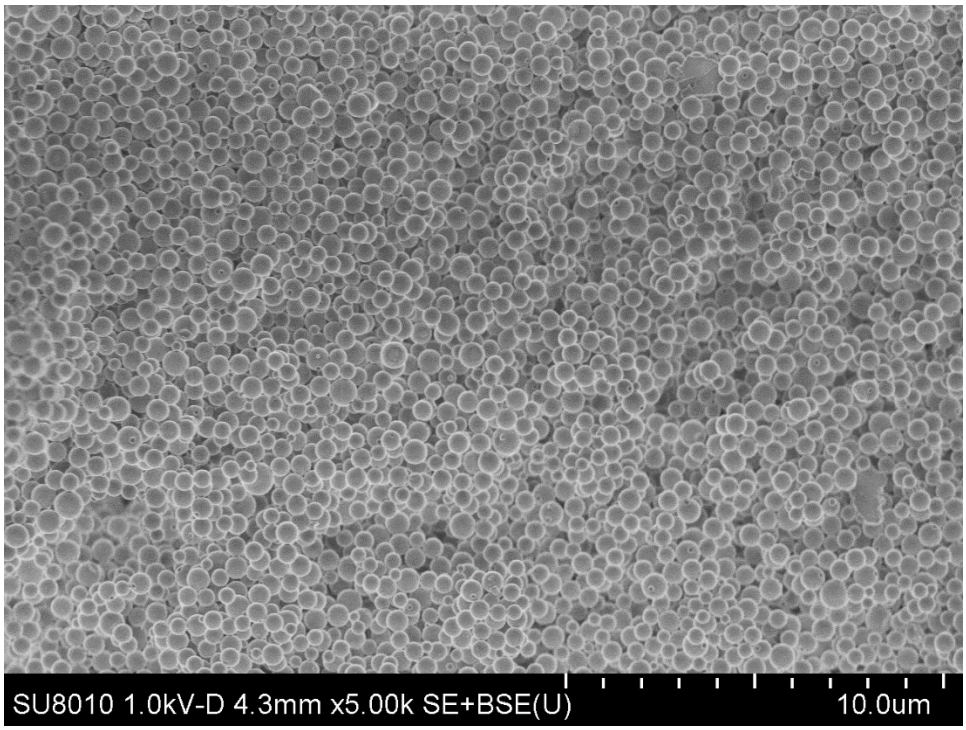

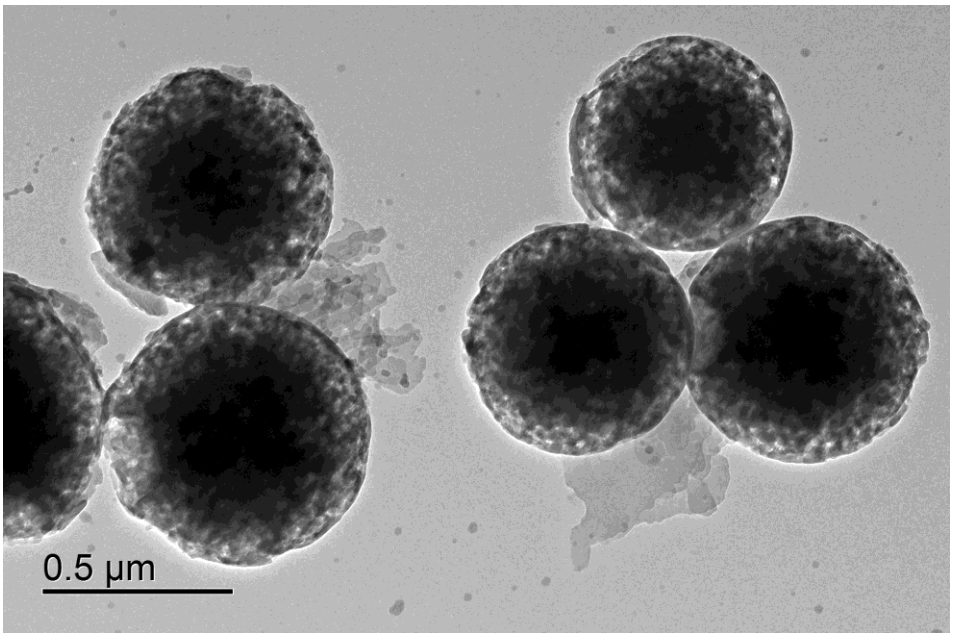

Fig. S18 SEM (a) and TEM (b) images of the precipitate of **MH** from THF/H_2O (1:99, v/v).

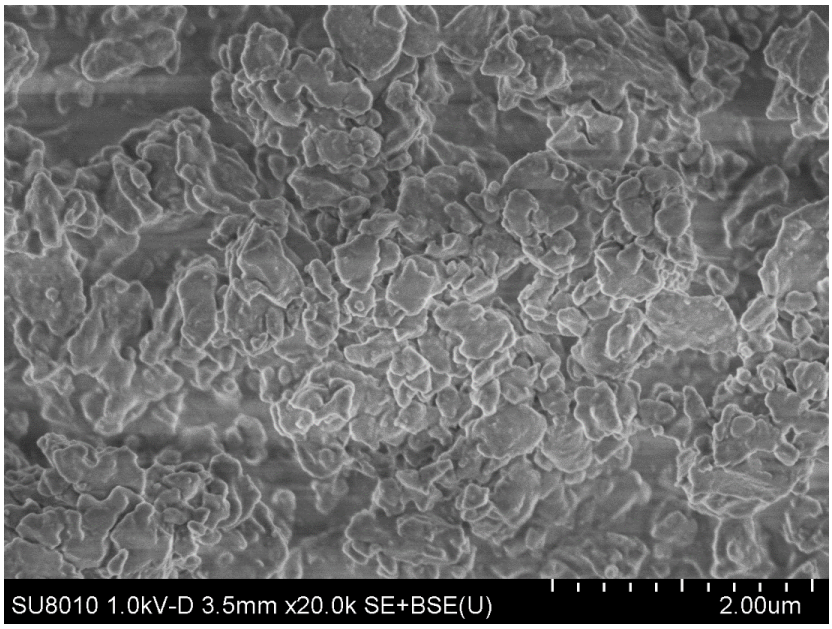

a)

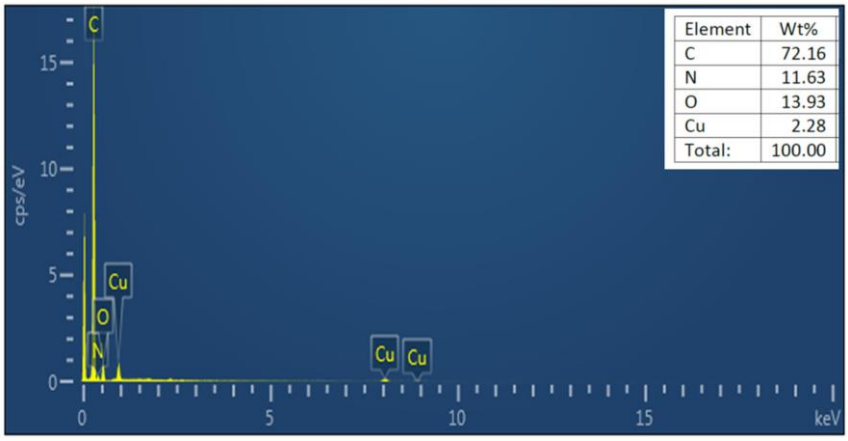

b)

Fig. S19 SEM (a) and EDS (b) images of the precipitate of **MH**/Cu^{2+} from THF/H_2O (1:4, v/v).

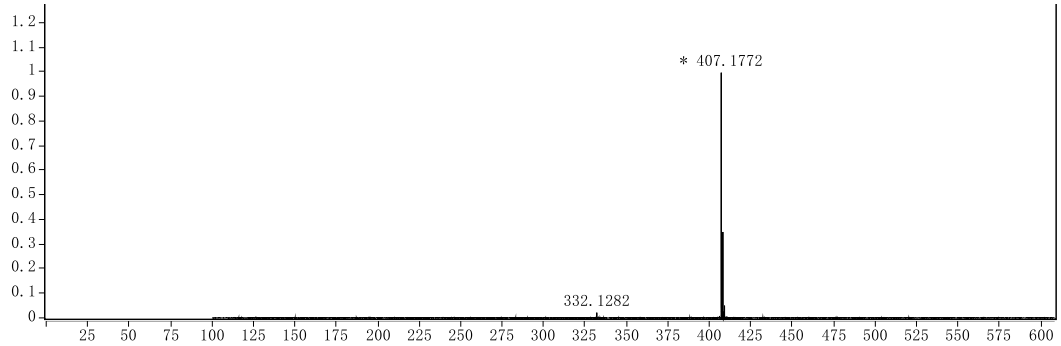

Fig. S20. MS spectrum of **L**.

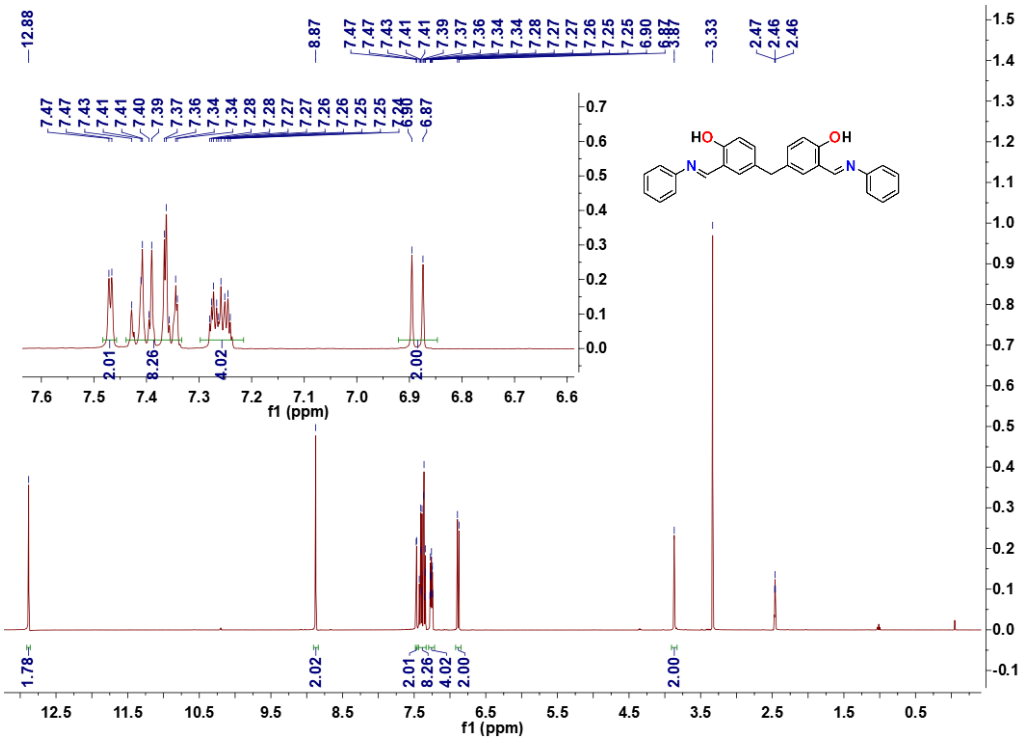

Fig. S21 ^{1}H NMR (400 MHz, DMSO-d_6) of **L**.

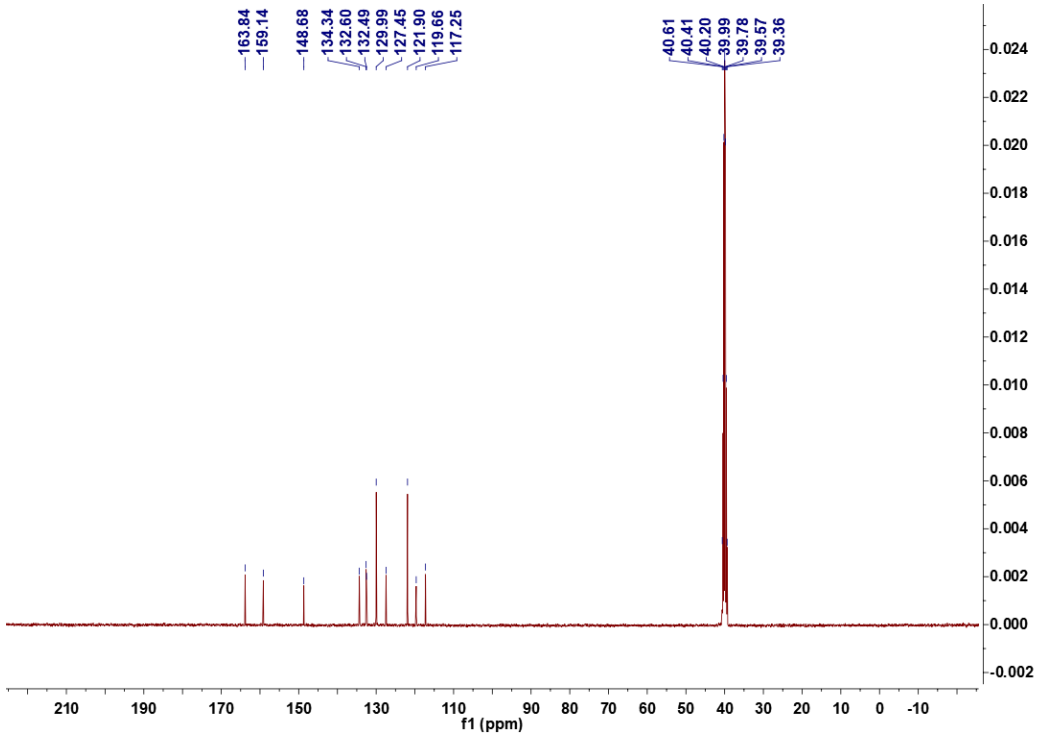

Fig. S22 ^{13}C NMR (100 MHz, DMSO-d_6) of **L**.